

The effects of earthquake source complexities on far-field source spectra

B. Halldorsson

Earthquake Engineering Research Centre, University of Iceland, Selfoss, Iceland

A.S. Papageorgiou

University of Patras, Patras, Greece



SUMMARY:

The Specific Barrier Model (SBM) is a particular case of a composite earthquake source model where the seismic moment is distributed in a deterministic manner on a rectangular fault plane on the basis of moment and area constraints. Recently, we have investigated variations of the SBM where we (a) allow subevents of different sizes, and (b) consider different isochron distributions on the earthquake fault. In this study we expound on the combined effects of the above variations on far-field earthquake source spectra. We show analytic equations for the high-frequency limit of source acceleration spectra and examine the extent of the variation that can be expected for high-frequency source spectra levels. We find that the isochrons also control the duration of strong-motion and the envelope of time-dependence of acceleration levels at a given site. The results shed light on the sources of variability of strong-motion amplitudes observed in earthquake data.

Keywords: specific barrier model, subevent size, isochron

1. INTRODUCTION

Earthquake source inversions have become prevalent in the scientific seismological literature over the last couple of decades. A common theme in the results of source inversions is the observed complexity of rupture, both in terms of nonuniform temporal and spatial distribution of slip on the fault plane for a single event (e.g., Custódio, Liu, & Archuleta 2005), and in terms of the intervariability of source processes between earthquakes (e.g., Mavroeidis & Papageorgiou 2010), and the inherent uncertainty of source parameters (Monelli & Mai 2008; Monelli *et al.* 2009). It has been found however that subevent structure of the main event is generally observed and this subevent structure is variable between earthquakes (Papageorgiou & Aki 1983a; Frankel 1991 p. 199; Aki 1992; Zeng, Anderson, & Yu 1994; Papageorgiou 2003; Mai, Spudich, & Boatwright 2005; Mavroeidis & Papageorgiou 2010). A simple earthquake source model that incorporates basic complexity is the specific barrier model, introduced and developed by Papageorgiou & Aki (1983a; b). It can be visualized as shown in Figure 1.1a, where subevents of equal diameter ($2\rho_0$, the ‘barrier interval’) are distributed on a rectangular fault plane without overlap. Papageorgiou (2003) has pointed out that the specific barrier model is a gross idealization of the faulting process of an earthquake. For example, the simplifying requirement of the subevents being of the same size may not hold and a population of different size subevents may be more realistic and result in a more appropriate description of the radiated seismic energy from the composite source, in accordance with results from source inversions [e.g., Papageorgiou & Aki, 1983a; Gusev, 1983, 1989; Joyner & Boore, 1986; Frankel, 1991; Zeng *et al.* 1994; Tumarkin *et al.*, 1994; Anderson, 1997]. Recently, Halldorsson & Papageorgiou (2012a; b) have quantified the effects on the expected far-field acceleration source spectra of such variations of the SBM. In this study we expound on their results by giving analytic equations for the high-frequency limit of source acceleration spectra of composite earthquake sources and examine the extent of the variation that can be expected for high-frequency source spectra levels. We discuss how the isochrons also control the duration of strong-motion and the envelope of time-dependence of acceleration levels at a given site. The results shed light on the sources of variability of strong-motion amplitudes observed in earthquake data.

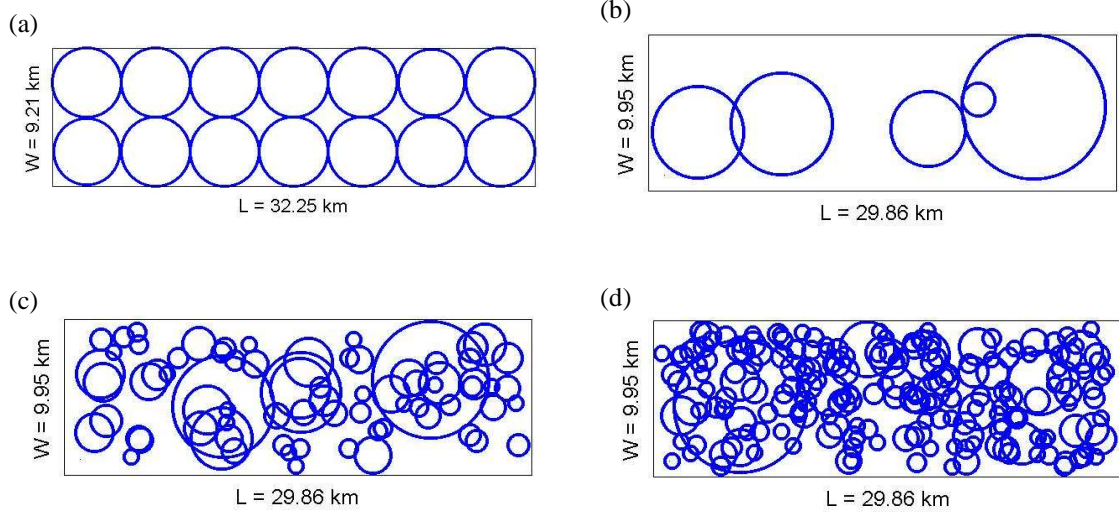


Figure 1.1. Examples of the rectangular fault plane of a composite earthquake source of magnitude $M_w 6.5$ for which the subevent population exhibits increasing complexity, manifested by subevents of increasingly different sizes. In the examples shown the subevents follow a (a) Dirac-delta probability density function (PDF) of subevent sizes (i.e., equal size subevents) that are arranged on the fault plane without overlap (i.e., the specific barrier model); (b) constant PDF; (c) fractal PDF with dimension $D = 2$; and (d) fractal PDF with dimension $D = 3$. In plots (b) to (d) the subevents are arranged randomly allowing overlap and their radii are allowed to vary over the range of $r = [0.05R_C; 0.5R_C]$ where R_C is the equivalent radius of the main earthquake event when modeled as a circular fault.

2. THE SEISMIC SPECTRUM OF A COMPOSITE EARTHQUAKE SOURCE

For completeness we list the basic premise of the approach of Halldorsson & Papageorgiou (2012a; b) and by consider the general case of a composite earthquake event composed of N circular subevents that vary in size (i.e., variable diameter). The radius of each subevent can take a random value in the range of $[R_a; R_b]$ that relate to R_C , the radius of the main event modeled as a circular crack, through the parameters α_1 and α_2 ($0 \leq \alpha_1, \alpha_2 \leq 1$) according to

$$\begin{aligned} R_b &= \alpha_1 R_C \\ R_a &= \alpha_2 R_b = \alpha_1 \alpha_2 R_C \end{aligned} \quad (1.1)$$

Subevent radii take values within this range according to a pre-scribed probability distribution. We apply the natural moment constraint that the cumulative seismic moment of the subevents equal the seismic moment of the main event. Seismic energy is radiated from the subevents as they rupture statistically independent of one another. The seismic energy radiated from all subevents that compose the main event arrives at a site over a time window of duration T_0 . Furthermore, the seismic energy radiated by subevent j ($j = 1 \dots N$) arrives at the site at random time instant T_j , where $0 < T_j < T_0$. We refer to T_j 's as the 'arrival times'.

On the basis of several simplifying assumptions of the interdependence of the random variables, we arrive at the expectation of the squared absolute value of the Fourier amplitude of the far-field spectrum of a composite source that consists of N subevents of random sizes R , where R is a random variable (Joyner & Boore 1986)

$$E[|S(\omega)|^2] = N \cdot E[|S_R(\omega, R)|^2] + N(N-1) \cdot |\tilde{f}_T(\omega)|^2 \cdot \{E[|S_R(\omega, R)|]\}^2 \quad (1.2)$$

where $S_R(\omega, R)$ is the subevent seismic spectrum (identical for all subevents) and $|\tilde{f}_T(\omega)|^2$ is the squared modulus of the ‘characteristic function’ of the random variable T , which represents the arrival time (at a station/observation point) of the radiation emitted by a subevent rupture. Taking the square root of the above equation i.e., $|S_C(\omega)| = \sqrt{E[|S(\omega)|^2]}$, we obtain the Fourier amplitude of the far-field source spectrum of the composite source (see Joyner & Boore 1986, and in particular; Halldorsson & Papageorgiou 2012a; b).

Both terms on the right hand side of the aggregate spectrum in Equation (1.2) are dependent on the expected value of the subevent seismic spectrum. By assuming that the kinematics of the subevent rupture are described by the symmetric circular crack model proposed by Sato & Hirasawa (1973), and as in Papageorgiou (1988) we neglect unimportant details of the far-field spectrum, the far-field S -wave spectrum of a subevent is given by the “ ω -square” model

$$S_R(\omega, r) = \frac{M_{o_i}}{1 + (f/f_2)^2} \quad (1.3)$$

where for a subevent i , represented by a circular crack of random radius R on which a local stress drop, $\Delta\sigma_L$, takes place, the seismic moment is given by

$$M_{o_i} = \frac{16}{7} \Delta\sigma_L R^3 \quad (1.4)$$

and f_2 is the corner frequency of the subevent, given by

$$f_2 = \frac{C_s \beta}{2\pi R} \quad (1.5)$$

where C_s is a model dependent and implicit function of the ratio v/β [$1.72 \leq C_s \leq 1.85$ for $0.7 \leq v/\beta \leq 0.9$] for the symmetric circular crack (Sato & Hirasawa, 1973; Aki & Richards, 1980), with β as the shear wave velocity in the vicinity of the source and v the ‘spreading velocity’ of rupture inside the circular cracks.

Traditionally seismic spectra in the far-field region have been interpreted using a circular crack model (e.g., Kanamori & Anderson 1975). From the (lowest) corner frequency (we refer to it as f_1) of such spectra one can estimate the dimension of the source, represented by the radius R_C of the crack model. The latter value, in combination with the seismic moment of the event, M_o^C , provides a stress drop measure, referred to here as ‘global stress drop’ $\Delta\sigma_G$. Following this convention, the composite source is represented by a circular crack of seismic moment equal to M_o^C , given by the expression

$$M_o^C = \frac{16}{7} \Delta\sigma_G R_C^3 \quad (1.6)$$

The parameter T_o is the duration of pulse-train (emitted by the subevents as they rupture) that is received at a station. An estimate of T_o may be obtained by calculating the duration of faulting of the composite source, which is inversely proportional to the (first) corner frequency of the source spectrum, $T_o = \tilde{C}/f_1$, where \tilde{C} is a model dependent constant (e.g., Silver 1983).

On the basis of the above formulation the far-field source acceleration spectrum of the SBM (see Figure 2.1a) was presented by Papageorgiou (1988). The expression is derived from Equation (1.2) and is

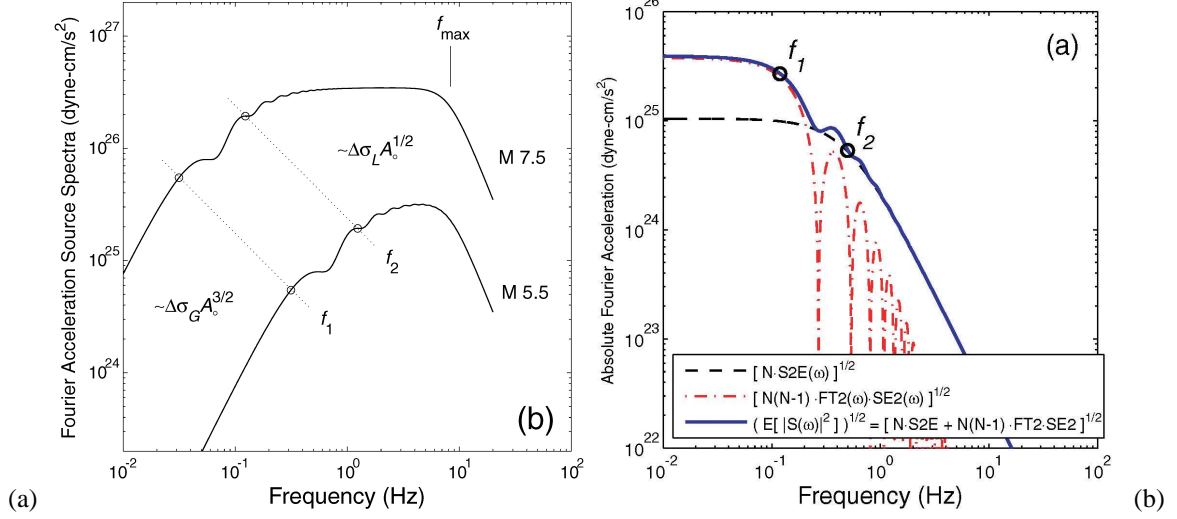


Figure 2.1. (a) Schematic view of the specific barrier model source acceleration spectra for two earthquake magnitudes, and the controlling parameters of the spectra over the frequency range. (b) Schematic view of the partition of the SBM displacement spectrum (blue) into the two terms on the right hand side of Equation (1.2). The example shown is for subevents of equal sizes (SBM) for which a single second corner frequency is defined.

$$S(M_o, f, \zeta) = \sqrt{N\zeta + N(N - \zeta) \left(\frac{\sin(\pi f T_0)}{\pi f T_0} \right)^2} (2\pi f)^2 \tilde{M}_{o_i}(f) \quad (1.7)$$

where we use f instead of circular frequency by convention, and ζ is a high-frequency source complexity factor introduced by Halldorsson & Papageorgiou (2005) (to account for the deviation of interplate source spectra from self-similar scaling). Halldorsson & Papageorgiou (2005), in recalibrating the SBM, have provided values for the global stress drop $\Delta\sigma_G$ based on the published literature, and the local stress drop $\Delta\sigma_L$ for three different tectonic regions on the basis of earthquake data. More recently, Foster *et al.* (2012) calibrated the SBM to the NGA dataset of interplate earthquakes.

We note that an inherent assumption in the above equation is that over the time window T_0 subevent seismic energy is assumed to arrive uniformly distributed. In other words, the probability density function (PDF) of energy arrival times at the station is

$$f_T(t) = \frac{1}{T_0}, \quad t \in [0; T_0] \quad (1.8)$$

The Fourier transform of $f_T(t)$ is denoted by $\tilde{f}_T(\omega)$, and is referred to as the ‘characteristic function’ of the R.V. T (Papoulis 1965). The squared amplitude of this characteristic function is

$$|\tilde{f}_T(\omega)|^2 = \sin^2\left(\frac{\omega T_0}{2}\right) / \left(\frac{\omega T_0}{2}\right)^2 \quad (1.9)$$

where $\omega = 2\pi f$ is the circular frequency. It is this function that appears in Equation (1.2)

We note that the left hand side of Equation (1.9) appears in Equation (1.2), and the right hand side appears in Equation (1.7). An important characteristic of Equation (1.9) is that it decays proportionally to ω^{-2} (Wyss & Brune 1967; Joyner & Boore 1986) and its limits as f approaches 0 and ∞ are one and zero, respectively (Papoulis 1965). Figure 2.1 shows how the displacement

spectrum expressed by Equation (1.2) is the summation of two dominant (at different ends of the spectrum) terms.

3. HIGH-FREQUENCY LIMIT OF THE SOURCE ACCELERATION SPECTRUM

The differences between the source spectra for various subevent size distributions can in part be quantified by their high-frequency spectral limits.

In the case of the SBM where all subevents are assumed to be of equal-size Equation (1.2) simplifies greatly to the form of

$$|S_C(\omega)| = \sqrt{N \left(1 + (N-1)|\tilde{f}_T(\omega)|^2\right)} \cdot |S_R(\omega, r_0)| \quad (1.10)$$

where r_0 is the subevent radius and $\zeta = 1$. By convention we prefer the notation ρ_0 for the subevent radius, as the ‘‘barrier interval’’ is $2\rho_0$. The SBM is a special case of a composite source where subevents of equal sizes are arranged on a rectangular fault plane without overlapping (Papageorgiou & Aki 1983a). This requires an additional area constraint, which results in the number of subevents of the SBM being

$$N = \left(\frac{\pi}{4}\right)^3 \left(\frac{\Delta\sigma_L}{\Delta\sigma_G}\right)^2 \quad (1.11)$$

The corresponding barrier interval is

$$2\rho_0 = \frac{4 \Delta\sigma_G}{\pi \Delta\sigma_L} 2R_C \quad (1.12)$$

We note that in terms of Equation (1.1) then for the SBM

$$\alpha_1 = \left(\frac{4}{\pi}\right) \left(\frac{\Delta\sigma_G}{\Delta\sigma_L}\right); \alpha_2 = 1 \quad (1.13)$$

The expressions for N and $2\rho_0$ along with Equations (1.3) to (1.6) and (1.9) fully define the seismic spectrum in Equation (1.7). We can therefore proceed to investigate its properties at low and high frequencies, respectively. The low-frequency limit of this displacement spectrum is

$$\begin{aligned} \lim_{\omega \rightarrow 0} |S_C(\omega)| &= \lim_{\omega \rightarrow 0} \sqrt{N(1 + (N-1)|\tilde{f}_T(\omega)|^2)} \cdot |S_R(\omega, r_0)| \\ &= N \lim_{\omega \rightarrow 0} |S_R(\omega, r_0)| = N \cdot M_{\circ_i} = M_{\circ} \end{aligned} \quad (1.14)$$

which is the total seismic moment, as expected, via the properties of the characteristic function and the subevent spectrum. The aggregate acceleration spectrum is then

$$|A(\omega)| = \omega^2 |S_C(\omega, r_0)| \quad (1.15)$$

and its high-frequency limit is therefore

$$\begin{aligned} \lim_{\omega \rightarrow \infty} |A(\omega)| &= \lim_{\omega \rightarrow \infty} \sqrt{N(1 + (N-1)|\tilde{f}_T(\omega)|^2)} \cdot |A(\omega, r_0)| \\ &= \sqrt{N} \omega_2^2 M_{\circ_i} \end{aligned} \quad (1.16)$$

where $\omega_2 = 2\pi f_2$ and $|A(\omega, r_0)| = \omega^2 |S_R(\omega, r_0)|$. The high-frequency limit can be written in various forms by making use of Equations (1.3) to (1.6). We note a couple of such result which equivalently show that

$$\begin{aligned} \lim_{\omega \rightarrow \infty} |A(\omega)| &\sim \Delta\sigma_L \sqrt{A_o} \\ &\sim \frac{1}{\sqrt{\alpha_1}} \sqrt{\frac{\Delta\sigma_L}{\Delta\sigma_G}} (\omega_1^2 M_o) = \left(\frac{\pi}{4}\right) \left(\frac{\Delta\sigma_L}{\Delta\sigma_G}\right) (\omega_1^2 M_o) \end{aligned} \quad (1.17)$$

where A_o is the fault area and $\omega_1 = 2\pi f_1$ is the circular corner frequency of the main event (as opposed to ω_2 for a single subevent) modeled as a circular crack.

In the case of subevent sizes following a uniform distribution between R_a and R_b , the high-frequency asymptote of the source acceleration spectrum can be calculated from Equation (1.2) keeping in mind the properties of the characteristic function. The result is

$$\lim_{\omega \rightarrow \infty} |A(\omega)| = \sqrt{N \frac{\alpha_1^2}{3} (\alpha_2^2 + \alpha_2 + 1)} \left(\frac{\Delta\sigma_L}{\Delta\sigma_G}\right) (\omega_1^2 M_o) \quad (1.18)$$

where the number of subevents in this case, N , is given by Equation (34) in Halldorsson & Papageorgiou (2012a).

Similarly, the case of a fractal distribution of subevent sizes between R_a and R_b , can be derived as

$$\lim_{\omega \rightarrow \infty} |A(\omega)| = \sqrt{N \frac{2\alpha_1^2 \alpha_2^2 \ln \alpha_2}{\alpha_2^2 - 1}} \left(\frac{\Delta\sigma_L}{\Delta\sigma_G}\right) (\omega_1^2 M_o) \quad (1.19)$$

for fractal dimension $D = 2$, in which case the number of subevents appearing in the above result is given by Equation (40) in Halldorsson & Papageorgiou (2012a). Alternatively, for fractal dimension $D = 3$, the high-frequency limit of the source acceleration spectrum is

$$\lim_{\omega \rightarrow \infty} |A(\omega)| = \sqrt{N \frac{3\alpha_1^2 \alpha_2^2}{2\alpha_2^2 + \alpha_2 + 1}} \left(\frac{\Delta\sigma_L}{\Delta\sigma_G}\right) (\omega_1^2 M_o) \quad (1.20)$$

where this time the number of subevents is given by Equation (41) in Halldorsson & Papageorgiou (2012a). As can be seen from the Equations (1.17) to (1.20) they share a common factor of $\omega_1^2 M_o$ which carries the properties of the main event (note also that the different N appearing in Equations (1.18) to (1.20) depend on stress drop ratios). While expressing their relative differences involves extensive algebra, Halldorsson & Papageorgiou (2012a) instead expressed graphically the relative differences between the above high-frequency spectral acceleration levels for each distribution type, relative to that of the SBM, for selected values of α_1 and α_2 , and stress drop ratios. We note that when the subevent size range becomes progressively narrower around the barrier interval (i.e., when $\alpha_2 = 1$ and $R_b = \alpha_1 R_c$ where $\alpha_1 = (4/\pi)(\Delta\sigma_G/\Delta\sigma_L)$) Equations (1.18) to (1.20) all have the same high-frequency limit, as is expected.

4. EFFECTS OF SOURCE-SITE GEOMETRY ON THE FAR-FIELD SPECTRA

Halldorsson & Papageorgiou (2012b) used the SBM to model earthquake sources of M_w 5.5, 6.5 and 7.5, respectively. They postulated two different rupture types on each source: (a) unilateral, and (b)

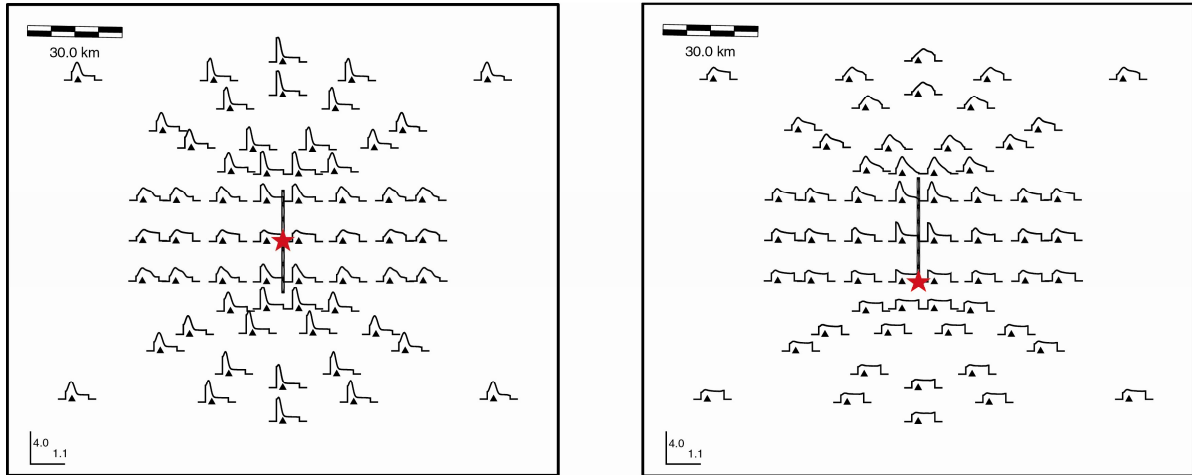


Figure 4.1. The normalized probability density functions of the energy arrival times plotted on a map of the hypothetical sites (triangles) located around the SBM representing a M_w 6.5 earthquake on a near-vertical fault on which a bilateral (*left*), and unilateral (*right*) rupture takes place. The the star denotes the epicentral location and the *solid lines* the surface projection of the fault

bilateral rupture, respectively. They used different aspect ratios L/W for each near-vertical fault plane configuration to account for the effects of a limited seismogenic width in shallow crustal interplate regions. By assuming a circular rupture front spreading with the speed of 0.75β on the fault plane from the rupture initiation point they synthesized, for a grid of hypothetical stations surrounding the earthquake fault, the respective isochrons on the fault plane as experienced by an observer at each stations. An isochron, corresponding to a station, is the locus of points on the fault plane the (instantaneous/impulsive) radiations of which reach the station simultaneously. By analyzing the shape of histograms of energy arrival times at each station they established a PDF of energy arrival times for each station on the hypothetical grid. In this way, they exhibited for the above earthquake sources and rupture types the physical manifestation of the probability distribution of energy arrival times at a station. Moreover, they grouped the prevalent and distinct types of PDFs, which equivalently constitute the shapes of the characteristic function that appears in the second term of the right hand side of Equation (1.2).

An example of the synthesized PDFs of energy arrival times in the *near-fault* region of a M_w 6.5 earthquake on a near-vertical fault and modeled by the SBM on which earthquake rupture takes place in the manner described above is shown in Figure 4.1. The plots shown in Halldorsson & Papageorgiou (2012b) depict the PDFs at *far-field* stations (except perhaps for the M_w 7.5 earthquake). We make the observation that for a given rupture type on the earthquake faults of different sizes the pattern of PDF shapes at the hypothetical stations is similar despite differences in earthquake sizes. The similarities can be described as follows for a *unilateral* rupture: The pattern is the same in all four quadrants that are defined by lines drawn along strike and strike-normal through the epicenter. At stations along the strike direction PDF shapes of group 4 are encountered. With increasing azimuthal angle away from strike the PDF shapes become smoother and approach those of group 2. The same pattern is observed for all earthquake sizes considered here. However, for a *bilateral* rupture the pattern is slightly more complicated. In the backward direction of rupture PDFs of group 1 are observed. PDFs of group 4 are only observed in the extreme near-fault region along the fault, and PDFs of group 3 are observed at stations in the forward direction away from the fault. Finally, in the fault-normal direction along the fault length at stations in the far-field region PDF shapes of groups 1-2 are observed. The dissimilarities in PDF shapes that arise are primarily due to the different aspect ratios of the earthquake faults. This becomes most evident for the M_w 7.5 earthquake source.

On the basis of the above observations we can predict with some degree of certainty what PDFs of energy arrival times are expected around an earthquake source of the type considered in this study,

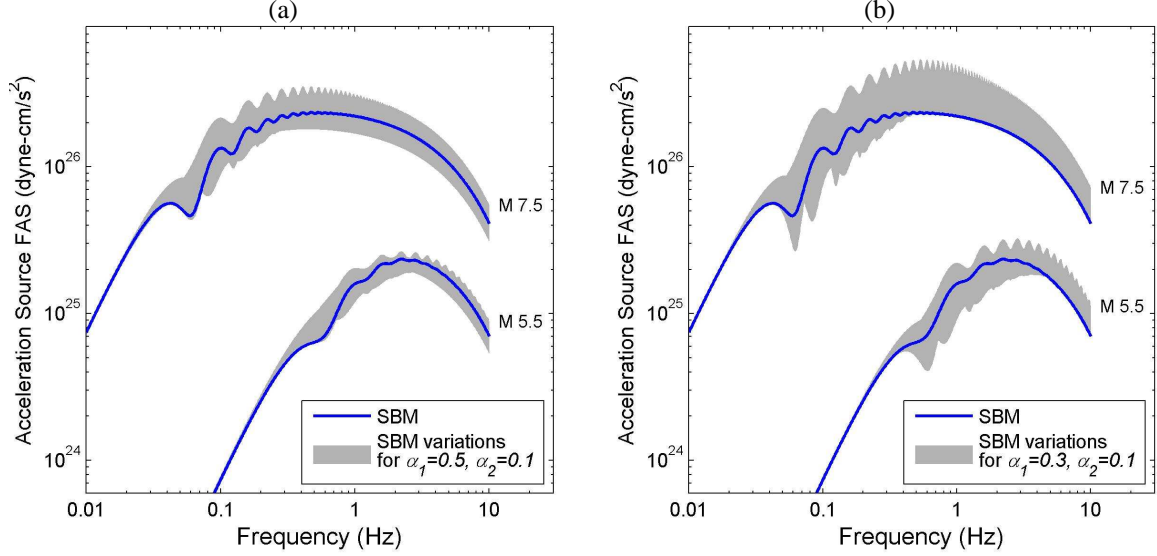


Figure 4.2. The combined effects of *variable size subevent* distributions and *isochron* distributions on the non-self-similar SBM earthquake source spectra (shown with high-frequency diminution effects, for $\kappa = 0.06$ s) for two earthquake magnitudes. The SBM source spectra are denoted by the blue curves. Subevents are allowed to vary in sizes between different values of the lower limit on subevent radii $R_a = \alpha_1 \alpha_2 R_C$ and upper limit of $R_b = \alpha_1 R_C$. The PDF of subevent sizes in this interval are allowed to be of all types considered by Halldorsson & Papageorgiou (2012a) (i.e., uniform, and fractal for both fractal dimensions 2 and 3). Additionally, the gray shaded region accounts for variable isochron effects on the source spectrum (Halldorsson & Papageorgiou, 2012b).

and that of Halldorsson & Papageorgiou (2012b). By estimating the absolute value of the Fourier transform of the function that gives rise to the PDF shape that is being considered at a station, the corresponding characteristic function can be evaluated. In fact, the characteristic functions of the PDFs of groups 1-4 are provided in the Appendix of Halldorsson & Papageorgiou (2012b) and are not repeated here.

The combined effects of variable size subevent distributions and isochron distributions on the non-self-similar SBM earthquake source spectra are shown in Figure 4.2 for two earthquake magnitudes. While the high-frequency level of the SBM acceleration spectrum is flat, according to Equation (1.7) we show the spectra (blue curves) with high-frequency diminution effects, based on $\Delta\sigma_L = 160$ bars and $\kappa = 0.06$ s (Foster *et al.* 2012). Namely, the gray shaded regions in Figure 4.2 show the extent of variation of the source spectral levels of a composite earthquake source where subevents are allowed to vary in sizes between the lower limit on subevent radii $R_a = \alpha_1 \alpha_2 R_C$ and upper limit of $R_b = \alpha_1 R_C$ where R_C is the equivalent radius of the main earthquake source, modeled as a circular crack. The PDF of subevent sizes in this interval are allowed to be of all types considered by Halldorsson & Papageorgiou (2012a) (i.e., uniform, and fractal for both fractal dimensions 2 and 3). Additionally, the gray shaded region accounts for variable isochrons effects on the source spectrum (Halldorsson & Papageorgiou 2012b). Plots (a) and (b) in the figure show the variations when very small subevent sizes are allowed ($\alpha_2 = 0.1$) and the maximum size of subevents is defined for $\alpha_1 = 0.5$ and 0.3, respectively. We observe from plot (b) that when the subevents are constrained to be smaller than the barrier interval much higher spectral amplitudes are seen, relative to plot (a). This is a consequence of a greater number of subevents being required to satisfy the seismic moment (especially for fractal size distribution). While the spectral variations in Figure 4.2 are seen to affect the frequency range down to the first corner frequency, the effects are due to different reasons at low and high frequencies, respectively. At intermediate frequencies (between first and second corner frequencies) the observed spectral variations combine the effects shown in Figure 4.1, namely the isochrons effects for stations surrounding a finite fault. As an example, we show in Figure 4.3 how the contribution to the spectral variations depends on the location of station relative to the fault rupture.

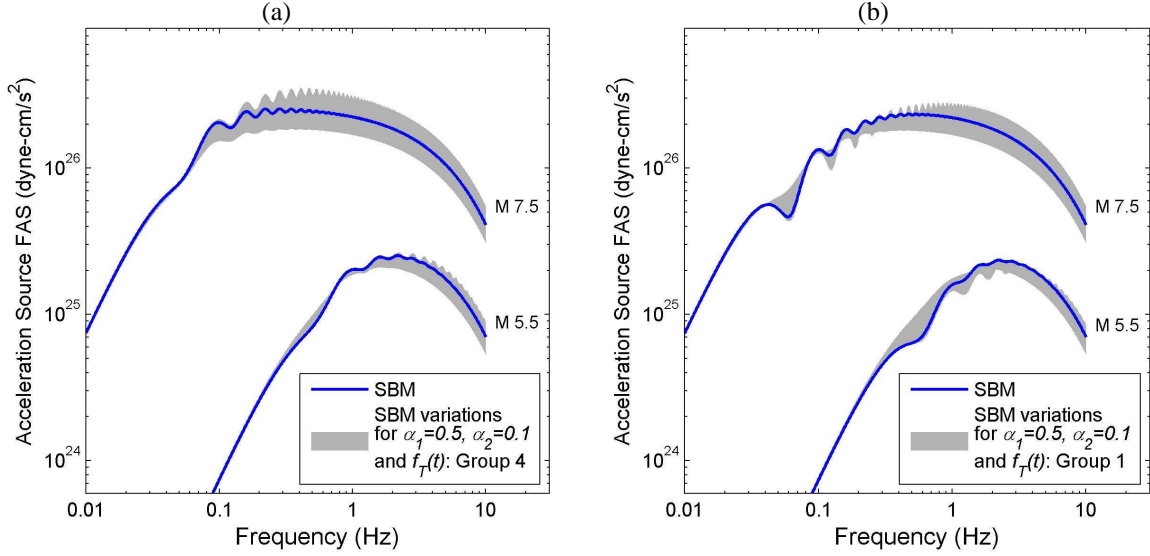


Figure 4.3. Same as in Figure 4.2a except the variation has been split into the effects for stations experiencing (a) forward directivity effects and (b) no directivity effects. The effect is primarily observed at intermediate frequencies.

5. DISCUSSION AND CONCLUSIONS

The combined effects of source complexity represented by variable size subevents and the different isochron distributions that each site experiences from simple models of rupture on near vertical faults as represented by the SBM and its variations manifests itself in variations of high-frequency source spectral amplitudes relative to the SBM. The results have not taken into account the effects of shorter/longer strong-motion duration for stations in the forward/backwards direction of rupture. Such effects would further elevate/lower the high-frequency levels shown here. The results shed light on the possible extent of contribution from source complexity and site-dependent isochron distributions on observed spectral amplitudes of ground motion spectra. Finally, the synthesized PDFs of arrival times around a finite source as modeled in this study can be used as ‘envelopes’ for shaping time histories of synthetic strong-motions in the context of the stochastic approach.

ACKNOWLEDGEMENT

This work was supported by Contract Numbers MCEER 00-0102, 01-0102, 02-0102, 03/0.1, and 04-0001 under the auspices of the Multidisciplinary Center for Earthquake Engineering Research (MCEER), Buffalo, New York; the United States National Science Foundation, Award Number EEC-9701471; the Icelandic Centre for Research (RANNIS) Project Grants No. 60043021, 90049021/22/23.

APPENDIX

We note a minor error in the Appendix of Halldorsson & Papageorgiou (2012b). The closed form equation for the characteristic function shown in Equation (16) in their Appendix is incorrect. The correct equation is

$$\begin{aligned}
 f(t) = \frac{1}{\omega^4} [& 2a^2 + 2T_0ab\omega^2 \\
 & - 2T_0a^2\omega \sin(T_0\omega) + 2b^2\omega^2 + T_0^2a^2\omega^2 \\
 & - 2\cos(T_0\omega)(a^2 + T_0ab\omega^2 + b^2\omega^2)]
 \end{aligned}
 \tag{1.21}$$

REFERENCES

- Aki, K. (1992) Higher-order interrelations between seismogenic structures and earthquake processes. *Tectonophysics*, **211**, 1–12.
- Aki, K. & Richards, P.G. (1980) *Quantitative Seismology. Theory and Methods*. W. H. Freeman and Company, San Francisco, USA.
- Anderson, J.G. (1997) Seismic energy and stress-drop parameters for a composite source model. *Bulletin of the Seismological Society of America*, **87**, 85–96.
- Custódio, S., Liu, P. & Archuleta, R.J. (2005) The 2004 M_w 6.0 Parkfield, California, earthquake: Inversion of near-source ground motion using multiple data sets. *Geophysical Research Letters*, **32**.
- Foster, K.M., Halldorsson, B., Green, R.A. & Chapman, M.C. (2012) Calibration of the Specific Barrier Model to the NGA Dataset. *Seismological Research Letters*, **83**, 566–574.
- Frankel, A. (1991) High-Frequency Spectral Falloff of Earthquakes, Fractal Dimension of Complex Rupture, b Value, and the Scaling of Strength on Faults. *Journal of Geophysical Research*, **96**, 6291–6302.
- Gusev, A.A. (1983) Descriptive statistical model of earthquake source radiation and its application to an estimation of short-period strong motion. *Geophysical Journal of the Royal Astronomical Society*, **74**, 787–808.
- Gusev, A.A. (1989) Multiasperity fault model and the nature of short-period subsources. *Pure and Applied Geophysics*, **130**, 635–660.
- Halldorsson, B. & Papageorgiou, A.S. (2005) Calibration of the Specific Barrier Model to Earthquakes of Different Tectonic Regions. *Bulletin of the Seismological Society of America*, **95**, 1276–1300.
- Halldorsson, B. & Papageorgiou, A.S. (2012a) Variations of the specific barrier model - Part I: Effect of subevent size distributions. *Bulletin of Earthquake Engineering*, Doi: 10.1007/s10518-012-9344-0.
- Halldorsson, B. & Papageorgiou, A.S. (2012b) Variations of the specific barrier model - Part II: Effect of isochron distributions. *Bulletin of Earthquake Engineering*, Doi: 10.1007/s10518-012-9345-z.
- Joyner, W.B. & Boore, D.M. (1986) On Simulating Large Earthquakes by Green's Function Addition of Smaller Earthquakes. *Earthquake Source Mechanics* Maurice Ewing Series. (ed S. Das), pp. 269–274. American Geophysical Union.
- Kanamori, H. & Anderson, D.L. (1975) Theoretical basis of some empirical relations in seismology. *Bulletin of the Seismological Society of America*, **65**, 1073–1095.
- Mai, P.M., Spudich, P. & Boatwright, J. (2005) Hypocenter Locations in Finite-Source Rupture Models. *Bulletin of the Seismological Society of America*, **95**, 965–980.
- Mavroeidis, G.P. & Papageorgiou, A.S. (2010) Effect of Fault Rupture Characteristics on Near-Fault Strong Ground Motions. *Bulletin of the Seismological Society of America*, **100**, 37–58.
- Monelli, D. & Mai, P.M. (2008) Bayesian inference of kinematic earthquake rupture parameters through fitting of strong motion data. *Geophysical Journal International*, **173**, 220–232.
- Monelli, D., Mai, P.M., Jónsson, S. & Giardini, D. (2009) Bayesian imaging of the 2000 Western Tottori (Japan) earthquake through fitting of strong motion and GPS data. *Geophysical Journal International*, **176**, 135–150.
- Papageorgiou, A.S. (1988) On two characteristic frequencies of acceleration spectra: Patch corner frequency and f_{max} . *Bulletin of the Seismological Society of America*, **78**, 509–529.
- Papageorgiou, A.S. (2003) The Barrier Model and Strong Ground Motion. *Pure and Applied Geophysics*, **160**, 603–634.
- Papageorgiou, A.S. & Aki, K. (1983a) A specific barrier model for the quantitative description of inhomogeneous faulting and the prediction of strong ground motion. I. Description of the model. *Bulletin of the Seismological Society of America*, **73**, 693–722.
- Papageorgiou, A.S. & Aki, K. (1983b) A specific barrier model for the quantitative description of inhomogeneous faulting and the prediction of strong ground motion. Part II. Applications of the model. *Bulletin of the Seismological Society of America*, **73**, 953–978.
- Papoulis, A. (1965) *Probability, Random Variables, and Stochastic Processes*. McGraw-Hill, New York.
- Sato, T. & Hirasawa, T. (1973) Body Wave Spectra from Propagating Shear Cracks. *Journal of Physics of the Earth*, **21**, 415–431.
- Silver, P. (1983) Retrieval of source-extent parameters and the interpretation of corner frequency. *Bulletin of the Seismological Society of America*, **73**, 1499–1511.
- Tumarkin, A.G., Archuleta, R.J. & Madariaga, R. (1994) Scaling relations for composite earthquake models. *Bulletin of the Seismological Society of America*, **84**, 1279–1283.
- Wyss, M. & Brune, J.N. (1967) The Alaska earthquake of 28 March 1964: A complex multiple rupture. *Bulletin of the Seismological Society of America*, **57**, 1017–1023.
- Zeng, Y., Anderson, J.G. & Yu, G. (1994) A composite source model for computing realistic synthetic strong ground motions. *Geophysical Research Letters*, **21**, 725–728.